Mechanical properties and microstructure of Ti6Al4V Extra Low Interstitial alloy produced via laser and electron beam additive manufacturing processes

E. Ghio, E. Cerri, M. Riccio, J. Sisti

The metal Additive Manufacturing technology is an innovative technology that allows flexibility in the sample design and optimized mechanical properties through the correct combination of the process parameters. The manufacturing of good and fully dense samples is fundamental to maximize tensile properties after appropriate heat treatments. This manuscript analyzes the microstructure and the mechanical properties of the Ti6Al4V-ELI heat-treated samples manufactured via Laser Powder Bed Fusion process (SLM Solutions). At the same time, it shows a comparative analysis of the same Ti6Al4VExtra Low Interstitial samples with other Ti6Al4V Extra Low Interstitial samples manufactured both via Laser Powder Bed Fusion (EOS machine) and via Electron Beam Melting in as built and heat-treated conditions. The microstructural analysis was conducted through optical and scanning electron microscopy, while the mechanical properties, obtained by the tensile and the Vickers microhardness tests, were compared to the ASTM F2924-14 and ASTM F136-13, respectively. The Ti6Al4V samples produced via laser powder bed fusion process (SLM Solutions) reaching 1040 ± 35 MPa and 975 ± 8 MPa of ultimate tensile strength and yield strength, respectively, and 11.1 ± 1% of elongation are placed between the laser powder bed fusion (EOS machine) samples and electron beam melted samples. Finally, it can be highlighted that the mechanical properties are related to the homogeneity, finesses, and size distribution of the β-phase at the α grain boundaries.

SOMMARIO

La tecnologia Additive Manufacturing è il punto focale di questo lavoro di ricerca. Una tecnologia innovativa che permette di avere flessibilità nella progettazione del campione e proprietà Meccaniche ottimizzate attraverso un'opportuna combinazione di parametri di processo. Solo stampando campioni completamente densi, le massime proprietà meccaniche possono essere ottenute dopo l'applicazione di appropriati trattamenti termici. In questo scenario, l'articolo analizza una la microstruttura e le proprietà meccaniche di campioni in Ti6Al4V-ELI trattati termicamente e prodotti per Laser Powder Bed Fusion. Nello stesso tempo, l'articolo mostra un'analisi comparativa della microstruttura e delle proprietà meccaniche dei campioni appena menzionati e di altri cam-

Emanuele Ghio, Emanuela Cerri
University of Parma, Department of Engineering and Architecture -
emanuele.ghio@unipr.it; emanuela.cerri@unipr.it;

Martina Riccio, Jacopo Sisti
Beam-IT, Strada Pinzera, 17, 43045, Fornovo di Taro, PR, Italy.

pioni di Ti6Al4V-Eli stampanti per Electron Beam Melting (EBM) e Laser Powder Bed Fusion (LPBF). L'analisi microstrutturale è stata Condotta tramite microscopia ottica ed elettronica, mentre le proprietà meccaniche, ottenuto da prove a trazione e test di microdurezza Vickers, sono state comparate rispettivamente con le normative ASTM F2924-14 e ASTM F136-13. I campioni di Ti6Al4V stampanti per LPBF raggiungendo 1040 ± 35 MPa e 975 ± 8 MPa di resistenza ultima a trazione e di snervamento rispettivamente, e 11.1-1% di allungamento a rottura si inseriscono tra i campioni stampati per LPBF ed Electron Beam Melting. È possibile sottolineare che le proprietà meccaniche sono correlate con l'omogeneità, finezza e distribuzione dimensionale della fase β ai bordi grano α.

INTRODUCTION

The Additive Manufacturing (AM) is the best process satisfying the requirements of the new industry revolution, also known as Industry 4.0, also considering the other subtractive manufacturing processes [1]. AM moves in opposite direction of these conventional manufacturing processes because it add material creating a 3D physical object through the "layer-by-layer" method [2]. At the same time, AM offers different advantages such as the freedom design, the manufacturing of sample having complex geometry and also characterized by a functionally-graded material, the reduction in time, cost production and in waste material. Finally, it synthesis the assembly process through the printing of a single part [1, 2, 3, 4]. Joining to these the personalization and customization, the AM technologies are the most suitable methods into the aerospace, automotive and biomedical sectors [1].

In relation to the machine set-up, namely the energy source rather than the material feed stock, the AM process is classified into powder bed fusion and direct energy deposition processes [2, 5]. Jimènez et al. [6] highlighted that the higher percentages of studies, research and especially the industrial use are related to the laser powder (31%) and electron beam powder bed fusion (17%) processes. The present paper enriches this scenario analysing two different processes based on the powder bed fusion method: the Laser Powder Bed Fusion (LPBF) performed through two different printing machines (EOS and SLM) and the Electron Beam Melting (EBM).

The first is based on the use of a laser beam that melts the powder bed layer, where the LPBF (EOS) induces lower thermal distortions and facilitates the melting process after the powder sinterizing [6]. In the second and last considered process, the electron beam source characterizing by a high voltage (30-60 keV) melts the powder bed into a high vacuum build chamber [7, 8]. The vacuum is necessary to avoid the printed sample oxidation and to keep the electron beam concentrated; moreover, it does not disperse energy due to the absence of gal molecules. On the other hand, argon or nitrogen gaseous are used to generate an inert environment within the build chamber in the LPBF processes [5]. In this scenario, the high reactivity of the titanium alloys with the oxygen makes the LPBF, and EBM process suitable to manufacture Ti6Al4V samples [8, 9].

Ti6Al4V is an α+β alloy due to the presence of ~ 6% and ~4% of Al and V stabilizing the α and β phases, respectively, and it is widely used into aerospace, automotive and biomedical fields due to its high corrosion resistance, low density, excellent biocompatibility, and high mechanical properties [10, 8, 9]. Generally, the as built microstructure of Ti6Al4V samples varies in relation to the manufacturing processes because the molten Ti solidifies with different cooling rates. Considering the LPBF samples, the presence of the acicular α' martensite phase, which crystallizes in hexagonal crystal system, brings the UTS (Ultimate Tensile Strength) and the YS (Yield Strength) values at ~1200÷1500 MPa and ~1100÷1200 MPa, respectively, while the elongation at ~ 5÷6% [11, 12, 13]. On the other hand, the as built electron beam melted (EBMed) samples that are formed by basketweave α+β microstructure where the α is a needle-like phase due to the cooling path (Figure 4), show a considerable decrease of the UTS and YS compared to the LPBF samples. The UTS reaches ~950÷1000 MPa, while YS ~850÷970 MPa as reported in [11, 14, 15]. Other authors have shown however the presence of the α' martensite in these samples caused by the not complete phase transformation α' → α + β [14, 16]. Moreover, the as built EBMed already show much lower internal residual stress than the as built LPBF samples due to the different process conditions and the obtained microstructure. Despite this, heat treatments above or below the β-transus (~ 980°C [17]) must be applied to reduce the internal stres-

ses and/or to dissolve the α′ martensite and so improving the ductility to 10% (the minimum elongation reported in F2924-14 specification) [18, 19, 20].

In the present manuscript, the ASTM F136-13 and the ASTM F2924-14 specifications were considered to evaluate the HV values and the tensile strength, respectively, reached after the heat treatments under the β-transus. In addition, the as built and heat-treated LPBF Ti6Al4V-ELI (Extra Low Interstitial) samples were compared with the same samples produced by another LPBF process and EBM and analyzed in [21].

MATERIAL AND METHOD

The gas atomized Ti6Al4V-ELI powder was used to manufacture the tensile samples analysed in the present manuscript. The chemical compositions of samples produced by the two LPBF investigated processes, commercially EOS (LPBF$_{EOS}$) and SLM Solution (LPBF$_{SLM}$), and EBM are shown in Table 1.

Tab.1 - Chemical compositions (weigth, %) of the Ti6Al4V-ELI powders used for the LPBFSLM process and for LPBFEOS and EBM [21] / Composizione chimica delle polveri (massa, %) di Ti6Al4V-ELI usate per i processi di LPBFSLM, LPBFEOS ed EBM [21].

	Ti	Al	V	O	N	H	Fe	C	Ref.
LPBF$_{SLM}$ SLM280HL	Bal.	5.5 − 6.5%	3.5 − 4.5%	< 0.1%	< 0.05%	< 0.011%	0.25%	< 0.08%	-
LPBF$_{EOS}$ EOS M290	Bal.	5.5 − 6.75%	3.5 − 4.5%	< 0.2%	< 0.05%	< 0.015%	< 0.3%	0.01	[21]
EBM	Bal.	6.47%	4.06%	0.09%	0.01%	0.001%	0.21%	0.01	

The dog-bone tensile samples (Figure 1a) analyzed in the present manuscript were manufactured via LPBF$_{SLM}$ process, with dimensions (Figure 1b) according to the ASTM E8/E8M standard [22]. The same geometry and printing configuration as drawn in Figure 1a (major axis parallel to the xy plane) was used for the samples analyzed in [21].
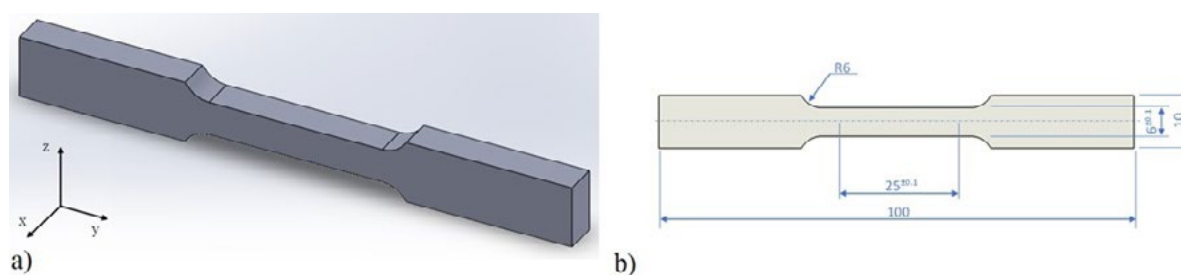
Fig.1 - a) 3D graphical representation of the dog-bone tensile sample. b) Dimensions of the dog-bone sample according to ASTM E8/E8M – 13a [31]. The sample thickness was 6 mm / Rappresentazione grafica 3D di un campione ad osso di cane. b) Dimensioni di un campione ad osso di cane in accordo con la normativa ASTM E8/E8M-13a [31]. Lo spessore del campione era di 6mm.

The LPBF$_{SLM}$ samples were fabricated with SLM Solutions SLM280HL dual machine using a 2x400 W IPG fiber lasers characterize by a spot size of 100 μm. The scan speed and the layer thickness used were 1250 mm/s and 60 μm, respectively. The entire process was performed in Ar atmosphere and using a pre-heated build platform at 80°C. For a better understating of this work, the process parameters used for the other samples are shown in Table 2.

Tab.2 - Process parameters used to manufacture the LPBF and EBMed samples / Parametri di processo usati per stampare i campioni tramite LPBF ed EBM.

Process parameters	LPBF$_{SLM}$	EBM, [21]	LPBF$_{EOS}$, [21]
Laser power [W]	400	-	400
Electron beam [keV]	-	60	-
Scan speed [mm/s]	1250	103	2000
Layer thickness [μm]	60	50	60
Spot laser size [μm]	100	-	100
Diameter electron beam [μm]	-	150-250	-
Build platform temperature [°C]	80	-	80
Chamber temperature [°C]	-	600	-

The SLMed as built samples were heat treated in a vacuum furnace at 740°C for 2h and subsequently cooled in two different steps. The former up to 530°C in 90min and the latter at room temperature in 1h using argon gas as shown in Figure 2. The same graph (Figure 2) shows the sche-matical representation of the heat treatment curve, which is described in [21], of the samples produced via LPBF$_{EOS}$ process. In the following part of this manuscript, 740/530 and 730/520 will be the heat treatments nomenclature.
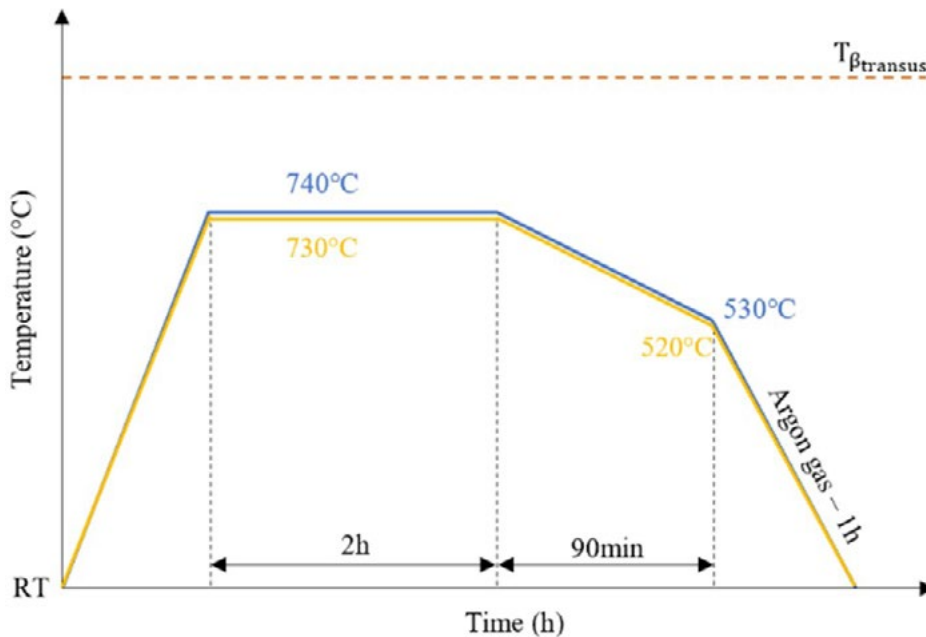
Fig.2 - Heat treatment schematic curves of the LPBF samples: blue curve is referred to the LPBF$_{SLM}$, while the yellow curve to the LPBF$_{EOS}$ / Curve di trattamento termico per i campioni prodotti per LPBFç la curva blu è riferita ai campioni LPBF$_{SLM}$, mentre quella gialla ai campioni LPBF$_{EOS}$.

The sample preparation for the metallographic analysis was performed on the resistant cross-section (xz plane) of the dog-bone sample and on the perpendicular surface (xy plane) to the build direction (z-axis). All polished surfaces were chemical etched with Keller's reagent. For the microstructural analysis was used Leica DMi8C reverse optical microscope and Nova NanoSEM 450 scanning electron microscope. In the last case, two different images (10000x) of the heat-treated samples were converted into binary images where the α-phase and the β-phase were distinguished into black and white regions, respectively. Subsequently, the binary images were analyzed through the LAS software (LAS AF V4.0) and each area, with its equivalent diameter, was determined. The results of the β-phase size distribution were discussed and then compared to those studied in [21].

The Leica VMHT microhardness tester was used to evaluate the microhardness values of the as built and heat treated LPBF$_{SLM}$ samples. Each value is obtained as an average of 10 measurements. The tests were carried out on the same polished surfaces where the microstructural analysis was conducted. For each measure the indentation time and the load applied were 15 s and 500 g, respectively, according to ISO 6507-1:2018.

The tensile properties of the SLMed samples were performed on 6 samples (Figure 1) using a Zwick-Roell Z100 machine with a relative strain rate of $8 \cdot 10^{-3}$ s^{-1}.

RESULTS AND DISCUSSION

Figures 3a,b shows the microstructure of the as built Ti6Al4V-ELI LPBF$_{SLM}$ sample along the build direction (Figure 3a) and on the xy plane (Figure 3b). The prior β-grains are characterized by a columnar shape and are directed along the heat fluxes involved during the molten pool solidification process. They are place almost perpendicular to the xy-plane of the build platform and, consequently to the molten pools as highlighted by the reciprocal position of the yellow (β-grains boundaries) and blue (molten pool boundaries) dotted lines (Figure 3a).
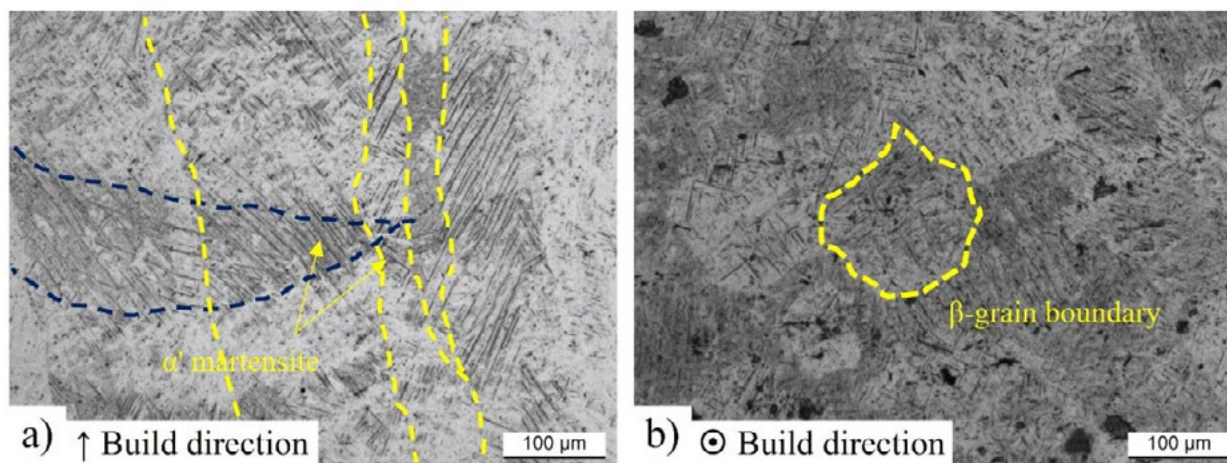
Fig.3 - Optical micrographs representing the xz (a) and xy (b) planes of the as built Ti6Al4V ELI sample. The yellow and blue dotted lines are related to the β-grains and molten pool boundaries, respectively / Micrografie ottiche che rappresentano i piani xz (a) ed xy (b) del campione as built di Ti6Al4V-ELI. Le line tratteggiate gialle e blu rappresentano rispettivamente i bordi dei grani β e dei molten pool.

The β-grains start from the bottom region of the sample and continue up to the top keeping parallel to the build direction (z-axis) regardless of the sample position into build chamber. This growth behavior is not only caused by the heat fluxes, but also by the columnar grains formed in the previous solidified layer ("n") that become the nuclei of formation and growth of the subsequent β-grains during the solidification of the next layer ("n+1") [23]. Focusing on xy plane (Figure 3b), it is possible to observe the typical equiaxed polyhedral shape of the columnar

grains. Due to the high cooling rate ($10^5 \div 10^7$ K/s), the microstruture of the as built Ti6Al4V-ELI is formed by fine acicular α' martensite highlighted by the yellow arrows in Figure 3a and contained into columnar grains. The LPBF induces a formation of the α' martensite phase due to the intersection between the light-blue curve and the Ms line as shown in Figure 4 where the cooling rate is > 410 °C/s.

As reported into the Handbook of titanium alloys, the line of the martensite start is at 800°C [24], while the β-transus at 980°C [17]. The grey dotted region (600-700 °C) represents the chamber temperature of the EBM process, and the green curve describes the cooling path characterizing the EBMed (Electron Beam Melted) samples.
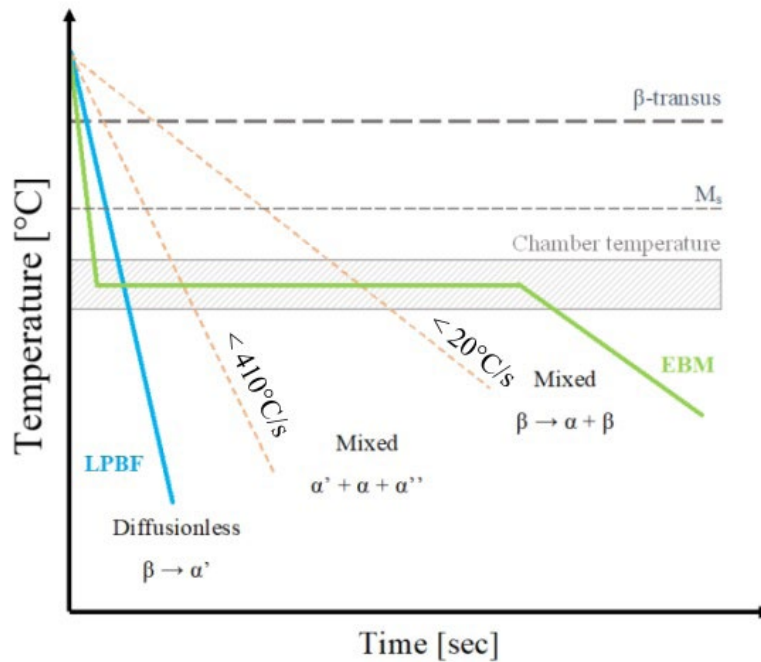
Fig.4 - Cooling paths (light-blue and green curves) referred to the different manufacturing processes and to the microstruture formed after the cooling at room temperature. The orange dotted lines are referred to the cooling rates <410°C/s and <20°C/s / Curve di raffreddamento (azzurra e verde) riferite a differenti processi di manifattura ed a microstrutture formate dopo i raffreddamenti a temperatura ambiente. Le linee tratteggiate arancioni sono riferite a raffreddamenti <410°C/s e <20°C/s.

Once again, the diffusionless transformation β → α' takes place due to the intersection with the Ms line; but the subsequent quasi-steady state at the chamber temperature (600 ÷ 700°C) induces a partial α' → α + β transformation time-temperature dependent [25, 26]. Gallaraga et al. [26] showed an as built microstructure formed by α+β phase using a chamber temperature of 650°C and after 36h and 40min of build time. Normally, at the end of this manufactured process, the samples slowly cooled at room temperature.

The orange dotted lines, however, represent the transfor-

mation into α' + α + α'' and β → α + β at cooling rate below the 410 °C/s and 20 °C/s, respectively.

Figure 5 shows the microstructure along the build direction of the heat-treated LPBF$_{SLM}$ samples (Figures 5a,d) after the 740/530, and LPBF$_{EOS}$ samples (Figures 5b,e) samples after the 730/520. Figures 5c,f show the microstructure of the EMBed samples in as built condition.
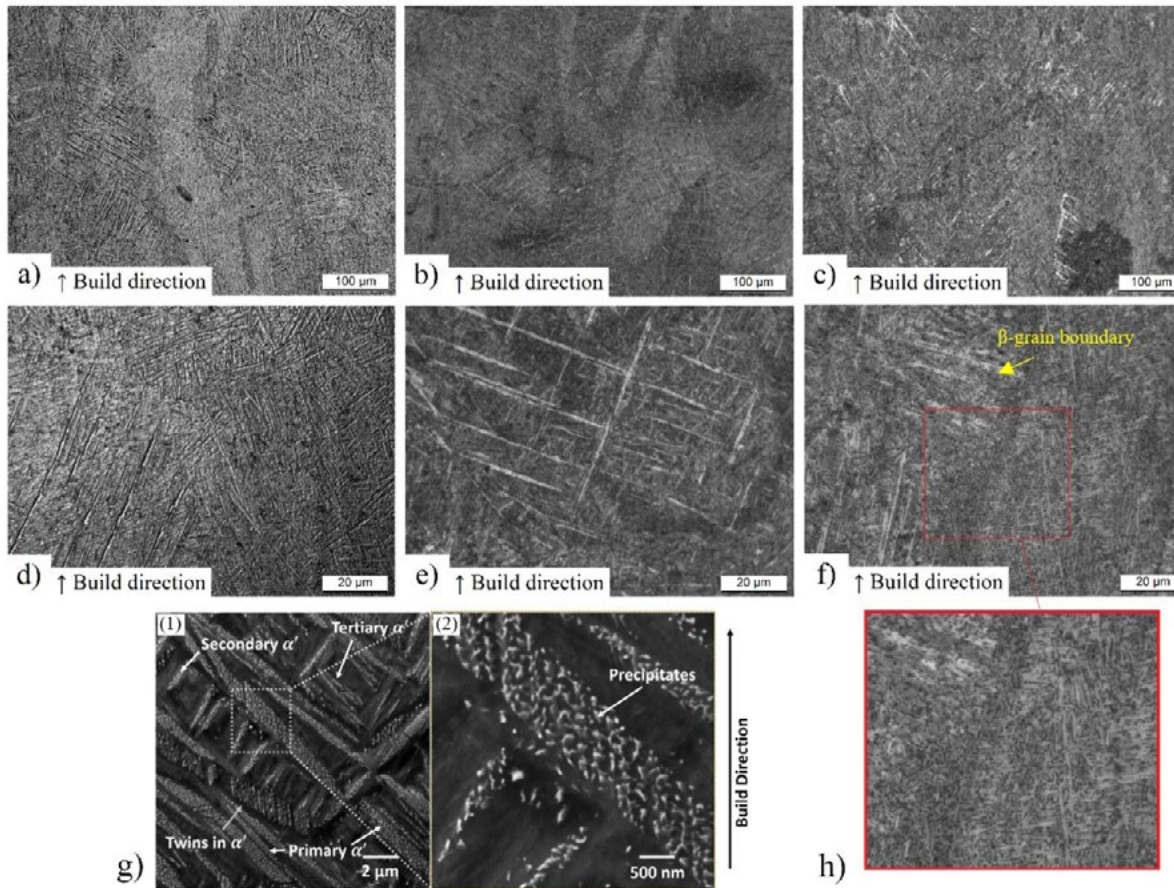
Fig.5 -Optical micrographs of the LPBF$_{SLM}$ samples (a, d), LPBFEOS samples (b, e) after the heat treatments: 740/530 (a, d) and 730/520 (b, e). (c, f) show the as built EBMed samples. g) (1) Example illustrating the hierarchical martensite structure of the as built SLMed Ti6A4lV sample where (2) is a magnification of (1) [27]. h) High magnification of a part of the optical micrograph in panel f / Micrografie ottiche di campioni di Ti6Al4V-ELI prodotti per SLM (a, d), DMLS (b, e) dopo trattamento termico: 740/530 (a, d) e 730/520 (b, e). (c, f) mostrano il campione prodotto per EBM g) (1) Esempio che illustra la struttura gerarchica della martensite di un campione as built di Ti6AL4V-ELI prodotto per SLM dove (2) è un ingrandimento di (1) [27]. h) Ingrandimento di una parte della micrografia in f

Comparing the different microstructures shown in Figures 5a-c, the columnar β-grains remain still visible even after 740/530 and 730/520 heat treatments showing that the LPBF manufacturing processes generated a columnar structure into the as built samples as well as the EBMed samples. For the SLMed samples, the columnar structures increase their thickness about 17%, while the α-phase, which is characterized by acicular and elongated shape (Figure 5d), reach values of thickness about 700 ± 10 nm due to the increase of about 40% after the 740/530. Figure 5e illustrates the microstructure of the LPBF$_{EOS}$ samples that is similar and more "cross-hatched" than the LPBF$_{SLM}$ microstructure (Figure 5c). It can be concluded that du-

ring the manufacturing process, not only the LPBF$_{SLM}$, but also the LPBF$_{EOS}$ process induce an α' martensitic nucleation and growth from the β-grains boundaries following a hierarchical structure (Figure 5g(1)). In addition, Figure 5g(2) shows the presence of fine precipitates within primary α'-martensitic laths [28]. Finally, comparing the high magnification micrograph (Figure 5f) representing the as built EMBed microstructure with the previously discussed Figures 5e,d, the α and β phases are differently distributed showing a typical basket-weave microstructure (Widmanstätten) as reported by [21]. In this microstructural configuration, the β-phase (dark domine in Figure 5h) separates the plate-like α-phase (bright area in Figure 5h)

and its amount reaches the 10% at room temperature. On the other hand, the quantity of the β-phase decreases to 5% and 4% respectively for the LPBF$_{EOS}$ and LPBF$_{SLM}$ sam-

ples. Consequently, the 90, 95 and 96% represent the percentage of the α-phase [21].
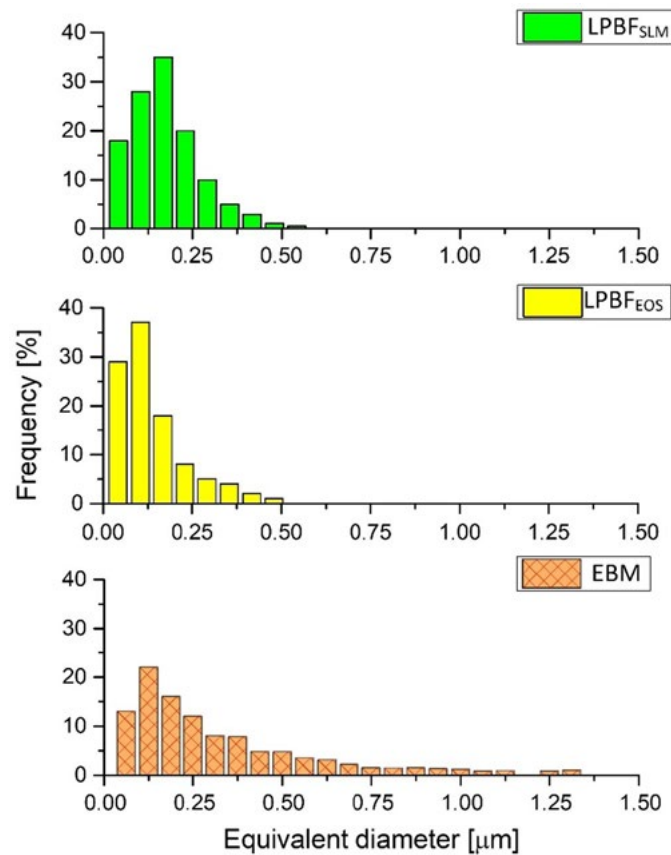
Fig.6 - Statistical distribution of the β-phase present into heat-treated LPBF$_{SLM}$, LPBF$_{EOS}$ and as built EMBed Ti6Al4V-ELI samples / Distribuzione statistica della fase β presente nei campioni trattati termicamente di Ti6AL-4V-ELI prodotti per LPBF$_{SLM}$,LPBF$_{EOS}$ e nei campioni prodotti per EBM.

Figure 6 shows the statistical distribution related to the β-phase equivalent diameter and at the first sight, the LPBF$_{SLM}$ (Figure 6a) and LPBF$_{EOS}$ (Figure 6b) samples show higher frequencies at the lower equivalent diameters than the EBMed samples (Figure 6c). Secondly, the LPBF$_{SLM}$ samples show a shift to the right of the maximum frequency peak with respect to the LPBF$_{EOS}$ samples that show 37% at 105 nm rather than 35% at 170 nm. So, the β-phases are more fragmented into the LPBF$_{EOS}$ than the LPBF$_{SLM}$ samples indicating that the α-phases are more "cross-hatched" in the former than in latter (Figure 5 e,f). The EBMed samples are instead characterized by the maximum peak of 22% at 125 nm, but also show equivalent diameters up to 1.3μm.
The mechanical properties of the different heat-treated LPBF samples and the as built EBMed samples are compared through both the Vickers hardness measurements

(Figure 7a) and the tensile properties (Figure 7b). The HV measurements performed on the three different planes of the LPBF$_{SLM}$ samples do not show great differences being that the values vary between 360 ± 5 HV$_{500}$ and 375 ± 8 HV$_{500}$. The same results are obtained considering the samples manufactured via LPBF$_{EOS}$ and EBM. In addition, considering the former (398 ± 4 HV$_{500}$) and the latter (345 ± 5 HV$_{500}$) manufacturing processes, the LBPF$_{SLM}$ samples are placed between them due to the different microstructures (Figure 5) and β-phase statistical distribution (Figure 6). On the other hand, the differences in terms of α-phase distribution, β-phase fragmentation and the different heat treatment can influence the variation between the LPBF$_{SLM}$ and LPBF$_{EOS}$ samples. All HV values are in agreement with the ASMT F136-13 specification.
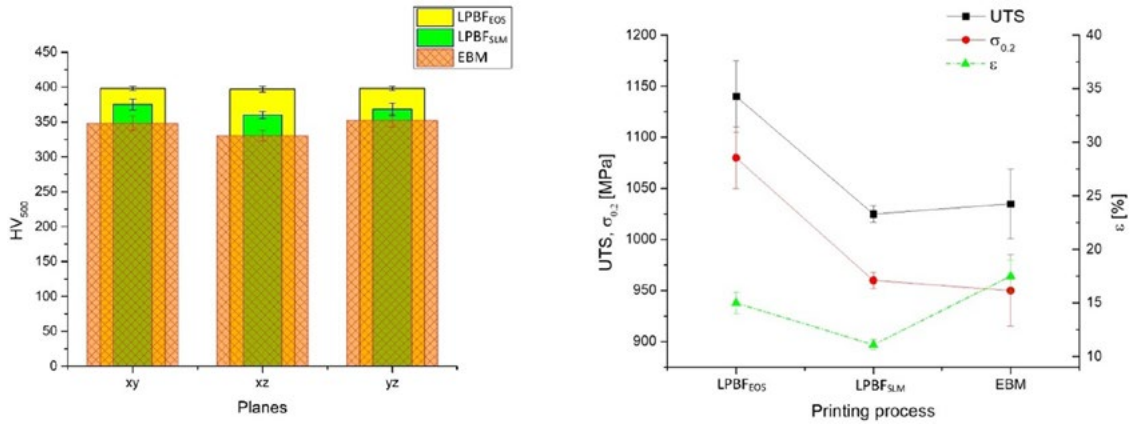
Fig.7 - Vickers microhardness values measured along the xy, xz and yz planes (a) and tensile properties (b) for the LPBF$_{SLM}$, LPBF$_{EOS}$ and EBMed TI6Al4V-ELI samples. / Valori di microdurezza Vickers misurati lungo i piani xy, xz e yz (a) e proprietà meccaniche (b) per i prodotti per LPBF$_{SLM}$ eLPBF$_{EOS}$.

As observed for the HV values, the tensile strengths show the same decreasing trends (Figure 7b) where the LPBF$_{SLM}$ samples reached 1040 ± 10 MPa and 975 ± 8 MPa for UTS and YS, respectively. The variation in terms of the elongation values between LPBF and EBM processes can be justified through the different microstructures in Figure 5 (Widmanstätten rather than the α-phase decomposed from the α' martensite) because the plastic deformation and cracks' propagation mechanisms take place differently as studied by [29]. Despite this, the tensile properties obtained by the LPBF$_{SLM}$, LPBF$_{EOS}$ and EBMed samples are in agreement with the ASTM F2924-14 specification and to other results shown in Table 3 where all considered conditions are formed by only one heat treatment step performed on as built samples as well as in Figure 2.

Tab.3 - Mechanical properties for Ti6Al4V samples manufactured with LPBF$_{SLM}$, EBM and LPBF$_{EOS}$ before and after heat treatments. The properties shown into ASTM F2924-14 are also reported. WQ = Water Quenching, AC = Air Cooling, FC = Furnace Cooling. / Proprietà meccaniche per campioni di Ti6Al4V stampati con processi di LPBF$_{SLM}$, EBM e LPBF$_{EOS}$ prima e dopo trattamento termico. Sono anche riportate le proprietà mostrate nella ASTM F2924-14. WQ = Tempra in acqua, AC = raffreddamento in aria, FC = raffreddamento in forno.

Process	Condition	UTS [MPa]	YS [MPa]	ε [%]	Cooling	Ref.
ASTM F2924-14	-	> 860	> 795	> 6 − 10	-	[20]
LPBF$_{SLM}$	As built	1246 ± 134	1150 ± 67	1.4 ± 0.5	-	[13]
	As built	1421 ± 120	1273 ± 53	3.2 ± 0.5	-	
	1050°C / 1h	984 ± 11	875 ± 36	7.4 ± 1.5	WQ	[17]
	950°C / 2h	1038 ± 30	935 ± 11	8.0 ± 1.5	WQ	
	700°C / 1h	1115-1116	1045-1054	9.5-12.4	AC	[30]
	600°C / 2h	956	907	10.8	AC	[31]
	730°C / 2	1067 ± 2	1003 ± 8	13.7 ± 0.4	FC	[32]
	800°C / 4h	1064 ± 2	990 ± 2	11 ± 0.8	FC	

800ºC / 4h	1026 ± 2	949 ± 2	5.5	FC	[33]
550ºC / 24h	1250	1150	4.5	-	
600ºC / 24h	1150	1100	6.0	-	
650ºC / 24h	1080	1020	5.5	-	
700ºC / 24h	1070	1010	4.2	-	
750ºC / 24h	900	880	3.0	-	
600ºC / 4h	700	650	2.4	-	
600ºC / 8h	1190	1125	6.0	-	
600ºC / 16h	1226	1140	4.0	-	
600ºC / 24h	1170	1130	6.0	-	
600ºC / 32h	1152	1115	5.8	-	[34]
482ºC / 6h	1130	1060	5.6	-	
482ºC / 8h	1130	1070	5.2	-	
482ºC / 10h	1125	1060	4.0	-	
704ºC / 4h	1125	1055	4.5	-	
704ºC / 5h	1040	980	5.7	-	
704ºC / 6h	1038	979	5.8	-	
788ºC / 3h	1029	981	5.7	-	
788ºC / 4h	980	950	5.9	-	
788ºC / 5h	1010	960	7.0	-	
800ºC / 4h	1001	952	7.6	-	
540ºC / 5h	1223 ± 52	1118 ± 39	5.36 ± 2.02	WQ	[11]
850ºC / 2h	1004 ± 6	955 ± 6	12.84 ± 1.36	FC	
850ºC / 5h	965 ± 20	909 ± 24	-	FC	
1020ºC / 2h	840 ± 27	760 ± 19	14.06 ± 2.53	FC	
705ºC / 2h	1082 ± 34	1026 ± 35	9.04 ± 2.03	FC	[35]
750ºC / 2h	1062	-	3.7	FC	
800ºC / 2h	1040	-	5.1	FC	
850ºC / 2h	1009	-	5.2	FC	
950ºC / 2h	970	-	10.1	FC	
1050ºC / 2h	945	-	11.6	FC	[36]
600ºC / 2h	1287	-	3.2	FC	
750ºC / 2h	1185	-	3.4	FC	
925ºC / 2h	988	-	12.2	FC	
1050ºC / 2h	980	-	9.2	FC	
750ºC / 2.5h	1200 ± 10	1100 ± 10	11 ± 1	FC	[37]
850ºC / 2.5 h	1180 ± 5	1020 ± 15	13 ± 1	FC	
920ºC / 2.5h	1020 ± 8	925 ± 10	15.1 ± 1.0	FC	
1050 ºC / 2.5h	1000 ± 10	830 ± 19	15.2 ± 1.2	FC	
920 ºC / 2.5h	1050 ± 10	870 ± 5	16 ± 1	FC	

EBM	As built	1117 ± 3	967 ± 10	8.9 ± 0.4	-	[29]
	As built	960 ± 2	850 ± 6	6.8 ± 0.5	-	[38]
	800°C / 2h	1000 ± 30	962 ± 30	5 ± 2	FC	[39]
	1000°C / 2h	945 ± 30	798 ± 30	11.6 ± 2	FC	
	1100°C / 0.5h	913 ± 38	774 ± 114	13 ± 2	FC	
	920°C / 2h	954	904	4.2	HIP[1] - FC	[40]
	1030°C / 2h	900	830	9.0	FC	
	1000°C / 3h	950	840	-	FC	[41]
	1050°C / 10h	975	850	-	FC	
	920°C / 2h	1005	900	14	HIP[2] - FC	[42]
	920°C / 2h	1000	905	12	FC	
LPBF$_{EOS}$	As built	~ 1158	~ 924	4-5.5	FC	[43]
	800°C / 4h	~ 1122	~ 805	12.6-16	FC	
	950°C / 1.5h	1083 ± 10	997 ± 35	-	FC	
	800°C / 4h	1060 ± 16	-	-	FC	[44]
	800°C / 4h	1191 ± 4	-	-	FC	

Correlating the HV and YS values of the LPBF$_{SLM}$ samples through the $\sigma_{0.2}$/HV ratio, the obtained value of 2.65 ± 0.04 is comparable to 2.71 ± 0.06 and 2.68 ± 0.05 obtained by the LPBF$_{EOS}$ and EBMed samples, respectively [21, 45]. In addition, these values are also in agreement with those found in literature varying from 2.20 to 2.90 [38, 46, 47].

In this manuscript, different heat-treated Ti6Al4V samples produced via LPBF$_{SLM}$, LPBF$_{EOS}$ and as built EBMed samples were considered, and their mechanical properties were analyzed. In this scenario, the Hollomon-Jaffe parameter (HP), also known as the Larson-Miller parameter, can describe the effect induced by the heat treatment on the Ti6Al4V samples as proposed by Chao et al. [48]. Originally, J.H. Hollomon [49] proposed the following time-temperature parameter to determine the effect induced by tempering heat treatment on the hardness of steels:

$$HP = T[\log(t) + C] \tag{1}$$

where T is the temperature expressed in K, t is the time expressed in h and C is a parameter referred to the material used [49]. Figure 8 shows the obtained correlation between the mechanical properties and the time-temperature parameter considering the result discussed in this work and all values shown in Table 3. The dotted blue line represents the time-temperature parameter related to the β-transus and considering a time of 1h. The different linear fits are reported as follows:

$$UTS_{(MPa)} = -0.0261 \, HP + 1538.4 \tag{2}$$
$$YS_{(MPa)} = -0.0309 HP + 1537 \tag{3}$$
$$\varepsilon\% = 7.82 \cdot 10^{-4} \, HP - 5.72 \tag{4}$$
$$HV = -3.7 \cdot 10^{-3} \, HP + 431.08 \tag{5}$$

and the best correlations are the Eqs. (1) and (2) due to the higher coefficient of correlations than the other ones as shown in Figures 8a-c, respectively. Figure 8c shows the elongation values where their high dispersion is caused by different factors which are related to the load direction of the tensile test and to the different microstructure obtained at room temperature.

---

[1]*Hot Isostatic Pressing heat treatment performed at 1000 bar [40].*
[2]*Hot Isostatic Pressing heat treatment performed at 1020 bar [42].*
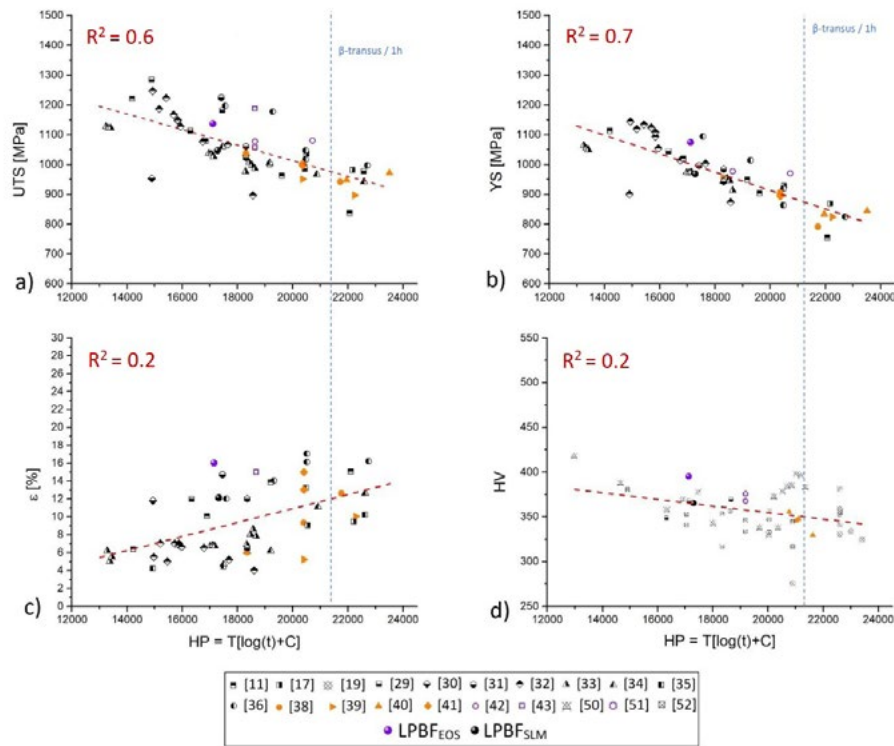
Fig.8 - Mechanical properties ((a) Ultimate tensile strength, (b) Yield strength, (c) Elongation, (d) Vickers microhardness) versus time-temperature parameter for heat-treated Ti6Al4V alloys manufactured via LPBF$_{SLM}$ and LPBF$_{EOS}$ processes. The costant C is equal to 15 [48]. The dottet blue line represent the time-temperature parameter related to the β-transus temperature (1000°C) and a time of 1h. The Vickers microhardness values are reported in [30, 32, 19, 50, 41, 51, 52, 53] / Proprietà meccaniche ((a) Carico di rottura, (b) Limite di snervamento, (c) Allungamento) rispetto al parametro di tempo-temperatura per le leghe Ti6Al4V trattate termicamente e prodotte tramite LPBF$_{SLM}$e LPBF$_{EOS}$. La costante C è uguale a 15 [44]. La linea blu tratteggiata rappresenta il coefficiente tempo-temperatura riferito alla temperatura di β-transus e al tempo di 1h.

Considering a subtransus heat-treated sample (T < T$_{β-transus}$, the columnar β-grains shape is not influenced and, consequently, the elongation can vary in relation to the load direction (Figure 9). Liu et al. [54] highlighted that the horizontal samples (Figure 9a) show lower elongations than the longitudinal samples (Figure 9b) due to the load distribution along with the different axis of the columnar β-grains and with different orientation of the α-phase. On the other hand, the α' martensite formed during the L-PBF process transforms into α+β in relation to the subtransus heat treatment temperature.
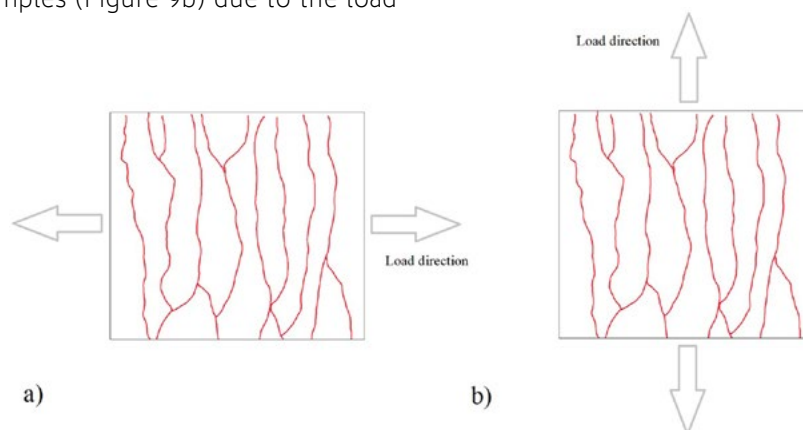
Fig.9 - Schematic representation of the columnar β-grains versus the load direction / Rappresentazione schematica dei grani colonnari β rispetto alla direzione del carico.

Vrancken et al. [11] emphasized that the α' → α+β transformation begins at 705°C and then, the α-phase tends to decrease from 87% at 780°C to 27% at 950°C. In this scenario, the residence time at these temperatures as the subsequent cooling method (water, air or furnace) do not influence incisively the grains growth because the α and β phases hinder each other [11]. On the other hand, the dislocation density and twin structures disappear as the temperature increases up to the β-transus. Tsai et al. [33] showed the presence of like-plate α and α'-martensite, which justify the low elongation obtained, after the heat treatments at 750 and 800°C for 24h (Table 3). The same authors show a considerable quantity of dislocations contained in the martensite. From the β-transus temperature the columnar β-grains are transformed in equiaxed grains, and the type of the α-phase is strictly related to the cooling method applied on the supertransus heat-treated samples (T>$T_{\beta-transus}$). After solubilization at 1050°C for 1h, followed by WQ, the diffusionless transformation of β-phase in new α' martensite occurs; while a furnace cooling induces a formation of a Widmanstätten microstructure with α+β colonies oriented in various directions [11, 17, 36]. The former microstructure induces a tensile strength improvement considering the subtransus heat-treated samples (800-900°C + AC/FC), except for the ductility. This is increased by the latter microstructural change due to the different mechanisms of slip and crack propagation as previously reported by comparing the samples produced via laser and electron beam additive manufacturing processes [29].

Finally, the presence of lack-of-fusion (LOF) pores can influence the ductility in relation to their position in the sample microstructure. The load directed perpendicularly to the LOF major axis tends to open it leading the sample to the premature failure. The other load configuration (parallel to the major axis) tends to close the pores not affecting the failure [54].

Other authors highlighted that the tensile strengths are increased at the expense of ductility due to the presence of the Ti_3Al precipitates [11]. This precipitation phenomenon can occur during the additive manufacturing process or during the aging heat treatment.

Figure 8d illustrates the Vickers microhardness in function of the HP parameter and, also in this case, any cor-

relation was not found due to the same consideration reported for the elongation. As matter of fact, the Vickers microhardness is most influenced by the microstructural inhomogeneity (fine, coarse or globular α-phase, presence of dislocation, α' martensite distribution, columnar or equiaxed β-grains) and presence of pores.

CONCLUSIONS

In the present paper, the $LPBF_{SLM}$ Ti6Al4V-ELI samples heat-treated at 740°C for 2h were compared to the $LPBF_{EOS}$ and EMBed Ti6Al4V-ELI samples. Generally, it can conclude as follows:

1. The as built $LPBF_{SLM}$ samples show a microstructure formed by columnar β-grains containing α'martensite. The columnar shape remains still visible after the heat treatment in $LPBF_{SLM}$, $LPBF_{EOS}$, And into as built EBMed samples.

2. The percentage of the β-phase observed into heat-treated $LPBF_{SLM}$ samples is 5% and, so, comparable to the $LPBF_{EOS}$ samples rather than the as built EBMed samples showing a Widmanstätten microstructure with a 10% of β-phase. Moreover, the $LPBF_{EOS}$ samples show higher β-phase fragmentation than the $LPBF_{SLM}$ samples probably due to the different scan speed and heat treatment.

3. The HV microhardness are isotropic into $LPBF_{SLM}$ samples as well as into the other samples, and the obtained values satisfied the ASTM F136-6 specification. The UTS of 1040 ± 10 MPa, the YS of 975 ± 8 MPa and the elongation at 11.1 ± 1% are in agreement to the ASTM F2924-14.

4. The Hollomon-Jaffe parameter can be used to determine the mechanical properties of heat-treated Ti6Al4V samples independently of the manufacture processes ($UTS_{(MPa)}$=-0.0261 HP +1538.4; $YS_{(MPa)}$= -0.0309 HP+1537). Vickers microhardness and elongation are not correlated with the HP parameter due to the microstructural complexity obtained after different heat treatments.

REFERENCES

[1]   J. Butt, «Exploring the Interrelationship between Additive Manufacturing and Industry 4.0,» Designs, vol. 4(2), p. 13, 2020.

[2]   W. Frazier, «Metal Additive Manufacturing: A review,» JMEPEG, vol. 23, pp. 1917-1928, 2014.

[3]   T. Maconiache, M. Leary, B. Lozanovsky, X. Zangh, M. Qian, O. Faruque e M. Brandt, «SLM lattice structures: Properties, performance, applications and challenges,» Mater. Des., vol. 183, p. 108137, 2019.

[4]   C. Zhang, F. Chen, Z. Huang, M. Jia, G. Chen, Y. Ye, Y. Lin, W. Liu, B. Chen, Q. Shen, L. ZHang e E. Lavernia, «Additive manufacturing of functionally graded materials: A review,» Mater. Sci. Eng. A, vol. 764, p. 138209, 2019.

[5]   T. Duda e L. V. Raghavan, «3D metal printing technology: the need to re-invent design practice,» AI & Soc, vol. 33, pp. 241-252, 2021.

[6]   A. Jemènez, P. Bidare, H. Hassanin, F. Tarlochan, S. Dimov e K. Essa, «Powder-based laser hybrid additive manufacturing of metals: a review,» The international Journal of Advanced Manufacturing Technology, vol. 114, pp. 63-96, 2021.

[7]   D. Gu, W. Meiners, K. Wissenbach e R. Propawe, «Laser additive manufacturing of metallic components: materials, processes and mechanisms,» Int. Mater. Rev., vol. 57, pp. 133-164, 2012.

[8]   M. Kolamroudi, M. Asmaael, M. Ilkan e N. Kordani, «Develompments on electron beam melting (EBM) of Ti-6Al-4V: A review,» Transaction of the Indian Istitute of Metals, vol. 74, pp. 783-790, 2021.

[9]   S. Kumar, T. S. Narayanan, S. Raman e S. eshadri, «Thermal oxidation of Ti6Al4V alloy: microstructural and electrochemical characterization,» Mater. Chem. Phys., vol. 119, pp. 337-346, 2010.

[10]   L. Murr, S. Quinones, S. Gaytan, M. Lopez, A. Rodela, E. Matrinez, D. hernandez, E. Martinez e F. M. R. Wicker, «Microstructure and mechanical behavior of Ti-6Al-4V produced by rapid-layer manufactured, for biomedical applications,» J. Mech. Behavior Bio. Mat., vol. 2, pp. 20-32, 2009.

[11]   B. Vrancken, L. Thjis, J. Kruth e J. Humbeeck, «Heat treatments of Ti6Al4V produced by Selective Laser Melting: Microstructure and mechanical properties,» J. All. Comp., vol. 541, pp. 177-185, 212.

[12]   K. Vanmeensel, K. Lietaert, B. Vrancken, S. Dadbakhsh, X. Li, J. Kurth, P. Krakhmalev, I. Yadroitsev e J. Humbeeck, «Additively manufactured metals for medical applications,» in Additive Manufacturing: Metarials, Processes, Quantifications and Applications, 2018, pp. 261-309.

[13]   B. Wysocki, P. Maj, R. Sitek, J. Buhagiar, K. Kurzydlowski e W. Swieszkowski, «Laser and electron beam additive manufacturing methods of fabricating titanium bone implants,» Appl. Sci., vol. 657, p. 7, 2017.

[14]   S. Al-Bermani, M. Blackmore, W. Zhang e I. Todd, «The origin of microstructural diversity, texture, and mechanical properties in Electron Beam Melted Ti-6Al-4V,» Metall. Mater. Trans. A, vol. 41, pp. 3422-3434, 2010.

[15]   J. Ran, F. Jiang, X. Sun, Z. Chen, C. Tian e H. Zhao, «Microstructure and mechanical properties of Ti-6Al-4V fabricated by electron beam melting,» Crystals, vol. 10(11), p. 972, 2020.

[16]   X. Tan, Y. Kok, W. Toh, Y. Tan, M. Descoins, S. Tor, K. Leong e C. Chua, «Revealing martensitic transformation and alpha/beta interface evolution in electron beam melting three-dimentional-printed Ti-6Al-4V,» Sci. Rep., vol. 6, pp. 1-10, 2016.

[17]   T. Vilaro, C. Colin e J. Bartout, «As-fabricated and Heat-treated microstructures of the Ti-6Al-4V alloy processed by Selective Laser Melting,» Met. Trans. A, vol. 42(A), pp. 3190-3199, 2011.

[18]   M. Villa, J. Brooks, R. Turner, H. Wang, F. Boitout e R. Ward, «Microstructural Modeling of the $\alpha + \beta$ Phase in Ti-6Al-4V: A Diffusion-Based Approach,» Metall. Mater. Trans. B., vol. 50, pp. 2898-2911, 2019.

[19]   P. Lekoadi, M. Tlotleng, K. Annan, N. Maledi e B. Masina, «Evaluation of heat treatment parameters on microstructure and hardness properties of high-speed Selective Laser Melted Ti6Al4V,» Metals, vol. 11, pp. 255-270, 2021.

[20]   Standard Specification for Additive Manufacturing Titanium-6 Aluminum-4 Vanadium with powder bed fusion., West Conshohocken, PA, USA, 2014.

[21]   E. Cerri, T. Rimoldi, R. Gabrini e L. Righi, «Investigation of microstructure and mechanical performance of Ti6Al4V-ELI components produced by DMLS and EBM additive technologies in different geometries,» La Metallurgia Italiana, vol. 4, pp. 32-43, 2019.

[22]   ASTM E8/E8M-13a: Standard test methods for tension testing of metallic materials, West Conshohocken - United Stases, 2013.

[23]   A. Antonysamy, J. Meyer e P. Pragnell, «Effect of build geometry on the β-grain structure and texture in additive manufacturing of Ti-6Al-4V by selective electron beam melting,» Mat. Charact., vol. 84, pp. 153-168, 2013.

[24]   R. Boyer, G. Welsh e E. Colling, Materials properties Handbook, ASM Internationalù, 1994.

[25]   A. Safdar, L. Wei, A. Snis e Z. Lai, «Evaluation of microstructural development in electron beam melted Ti-6Al-4V,» Mater. Charact., vol. 65, pp. 8-15, 2012.

[26]   H. Gallaraga, D. Lados, R. Dehoff, M. Kirka e P. Nandwana, «Effect of the microstructure and porosity of Ti-6Al-4V ELI alloy fabricated by electron beam melting (EBM),» Add. Man., vol. 10, pp. 47-57, 2016.

[27]   E. Ghio e E. Cerri, «Additive Manufacturing of AlSi10Mg and Ti6Al4V Lightweight alloys via laser powder bed fusion: A review of heat treatments effects,» Materials, vol. 15(6), p. 2047, 2022.

[28]   J. Yang, H. Yu, J. Yin, M. Gao, Z. Wang e X. Zeng, «Formation and control of martensite in Ti-6Al-4V alloy produced by selective laser melting,» Mat. Des., vol. 108, pp. 308-318, 2016.

[29]   M. Simonelli, Y. Tse e C. Tuck, «Effect of the building orientation on the mechanical properties and fracture modes of SLM Ti-6Al64V,» Mat. Sci. Eng. A, vol. 616, pp. 1-11, 2014.

[30]   G. Kasperovich e J. Hausmann, «Improvement of fatigue resistance and ductility of Ti6Al4V processed by Selective Laser Melting,» J Mat. Proc. Techn., vol. 220, pp. 202-2014, 2015.

[31]   F. Wang, J. Mei, H. Jiang e X. Wu, «Laser fabrication of Ti6Al4V/TiC composites using simultaneous powder and wire feed,» Mater. Sci. Eng. A., Vol. %1 di %2445-446, pp. 461-466, 2007.

[32]   S. Cecchel, D. Ferrario, G. Cornacchia e M. Gelfi, «Development of Heat Treatments for Selective Laser Melting Ti6Al4V Alloy: Effect on Microstructure, Mechanical Properties, and Corrosion Resistance,» Advanced Engineering Materials, 2020.

[33]   M. Tsai, Y. Chen, C. Chao, J. Jang, C. Tsai, Y. Su e C. Kuo, «Heat-treatment effects on mechanical properties and microstructure evolution of Ti-6Al-4V alloy fabricated by laser powder bed fusion,» J. Alloys Compound., vol. 816, p. 152615, 2020.

[34]   F. Nalli, L. Bottini, A. Boschetto, L. Cortese e F. Veniali, «Effect of industrial heat treatment on the mechanical performance of Ti6Al4V processed by Selective Laser melting,» App. Sci., vol. 10, pp. 2280-2296, 2020.

[35]   M. Thoene, S. Leuders, A. Riemer, T. Troester e H. Richard, «Influence of heat-treatment on Selective Laser Melting products – e.g. Ti6Al4V,» in Conference Proceedings and journals - International Solid Freeform Fabricartion Symposium, 2012.

[36]   A. Khorasani, I. Gibson, M. Goldberg e G. Littlefair, «On the role of different annealing heat treatements on mechanical properties and microstructure of selective laser melted and conventional wrought Ti-6Al-4V,» RPJ, vol. 23(2), pp. 295-304, 2017.

[37]   N. Jin, Z. Yan, Y. Wang, H. Cheng e H. Zhang, «Effects of the heat treatment on microstructrure and mechanical porperties of selective laser melted Ti-6Al-4V lattice materials,» International Journal of Mechanical Sciences, vol. 190, p. 106042, 2021.

[38]   M. Koike, P. Geer, K. Owen, G. Lilly, L. Murr, S. Gaytan, E. Martinez e T. Okabe, «Evaluation of Titanium Alloys Fabricated Using Rapid Prototyping Technologies—Electron Beam Melting and Laser Beam Melting,» Mater., vol. 4(10), pp. 1776-1792, 2011.

[39]   S. Leuders, M. Thoene, A. R. T. Niendorf, T. Troester, H. Richard e H. Maier, «On the mechanical behaviour of titanium alloy Ti6Al4V manufactured by selective laser melting: fatigue resistance and crack growth performance,» Inter. J. Fatig., vol. 48, pp. 300-307, 2013.

[40]   A. Syed, M. Awd, F. Walther e X. Zhang, «Microstructure and mechanical properties of as-built and heat-treated electron beam melted Ti–6Al–4V,» Materials Science and Technology, vol. 35, 2019.

[41]   S. Raghavan, M. Nai, P. Wang, W. Sin, T. Li e J. Wei, «Heat treatment of electron beam melted (EBM) Ti-6Al-4V: microstructure to mechanical property correlations,» RPJ, vol. 24(4), pp. 774-783, 2018.

[42]   O. Teixiera, F. Silva, L. Ferreira e E. Atzeni, «A review of heat treatments on improving the quality and residual stresses of the TI-6Al-4V parts produced by additive manufacturing,» Met., vol. 10(8), p. 1006, 2020.

[43]   Z. Mierzejewska, R. Hudak e J. Sidun, «Mechanical Properties and Microstructure of DMLS Ti6Al4V alloy dedicated to biomedical applications,» Mater., vol. 12, p. 176, 2019.

[44]   D. Srinivasan, A. Singh, A. Reddy e K. Chatterjee, «Microstructural study and mechanical characterisation of heat-treated direct metal laser sintered Ti6Al4V for biomedical applications,» Materials technology, 2020.

[45]   E. Cerri e E. Ghio, «AlSi10Mg alloy produced by Selective Laser Melting: Relationships between Vickers microhardness, Rockwell hardness and mechanical properties,» La Metallurgia Italiana, vol. 112, pp. 5-17, 2020.

[46]   H. Rafi, N. Karthik, H. Gong, T. L. Starr e B. Stucker, «Microstructures and Mechanical Propreties of Ti6Al4V parts fabricated by Selective Laser Melting and Electron Beam Melting,» JMEPEG, vol. 22, pp. 3872-3883, 2013.

[47]   F. Azam, A. Rani, K. Altaf, T. Rao e H. Zaharin, «An In-Depth review on direct additive manufacturing of metals,» in IOP Conference Series: Materials Science and Engineering, Batu Ferringhi, Penang, 2018.

[48]   Q. Chao, P. Hodgson e H. Beladi, «Thermal stability of an ultrafine grained Ti-6Al-4V alloy during post-deformation annealing,» Materials Science & Engineering A, vol. 694, pp. 13-23, 2017.

[49]   J. Hollomon, «Time-Temperature relations in tempering steel,» Trans. AIME, vol. 162, pp. 223-249, 1945.

[50]   S. Wu, Y. Lu, Y. Gan, T. Huang, C. Zhao, J. Lin, S. Guo e J. Lin, «Microstructural evolution and microhardness of selective-laser-melted Ti-6Al-4V alloy after post heat treatments,» J. All. Compound., vol. 672, pp. 643-652, 2016.

[51]   A. Guzanova, G. Izarikova, J. Brezinova, J. Zivcak, D. Draganovska e R. Hudak, «Influence if build orientation, heat treatment, and laser power on hardness of Ti6Al4V manufactured using the DMLS process,» Met., vol. 7(8), p. 318, 2017.

[52]   X. Zhang, G. Fang, S. Leeflang, A. Boettger, A. Zadpoor e J. Zhou, «Effect of subtransus heat treatment on the microstrucutre and mechanical properties of additively manufactured Ti-6Al-4V alloy,» J. All. Compound., vol. 735, pp. 1562-1575, 2018.

[53]   X. Yue, H. Fukazawa, K. Maruyama, K. Matsuo e K. Kitazono, «Effect of post pheat treatment on the mechanical properties of porous Ti-6Al-4V alloys manufactured through powder bed fusion process,» Materials transactions, vol. 60(1), pp. 74-79, 2019.

[54]   S. Liu e Y. Shin, «Additive manufacturing of Ti6Al4V alloy: A review,» Mat. Des. , vol. 164, p. 107552, 2019.